Journal of Materials Chemistry C

PAPER

View Article Online
View Journal | View Issue

Cite this: J. Mater. Chem. C, 2015, 3, 3714

Electronic properties of tin dichalcogenide monolayers and effects of hydrogenation and tension†

Shijie Wen,[a] Hui Pan*[a] and Yuebing Zheng[b]

Received 12th January 2015,
Accepted 13th February 2015

DOI: 10.1039/c5tc00093a

www.rsc.org/MaterialsC

Transition metal dichalcogenide monolayers have attracted extensive attention because of their rich physical and chemical properties and wide applications. In this work, we systematically investigate the electronic properties of tin dichalcogenide monolayers (SnX_2, X = S, Se, and Te) and the effects of hydrogenation and tension by first-principles calculations based on the density-functional theory. We find that a pure SnX_2 monolayer can be an intrinsic semiconductor or metal depending on the Sn–X bonding state. Hydrogenation can transfer its conductivity from a narrow-band semiconductor or a metal to wide-band semiconductor. We further show that a monolayer with a tunable band gap and even metallic characteristics can be achieved by applying tension. We predict that these tin-based dichalcogenide monolayers with controllable multi-functions may be employed in nanodevices and sensors.

I. Introduction

Two-dimensional (2D) monolayers, such as graphene and transition metal dichalcogenides, have attracted extensive attention because of their intriguing electronic, optical, magnetic, mechanical, chemical and biological properties and potential multi-functional applications.[1–13] The transition metal dichalcogenide monolayers (MX_2) are a class of sandwich 2D materials with X atoms at the top and bottom and M atoms in between.[4] Normally, M is a transition metal element from group IV, group V, or group VI, and X is a chalcogen (S, Se or Te). Different from graphene, 2D MX_2 can be metallic, semiconducting, nonmagnetic, and ferromagnetic due to the rich choice of compositions and phase transitions,[4,6,13–20] and it has been widely studied recently for its applications in nanodevices, catalysts, solar cells, lithium batteries, sensors, *etc.*[5,13,20–28] Importantly, its physical and chemical properties can be easily modified to satisfy particular application requirements by functionalization and an external field due to the excellent surface chemical activity and mechanic flexibility.[25–42] For example, it has been reported that the electronic and magnetic properties of 2D MX_2 can be efficiently tuned by external tension and controlled by hydrogenation.[9,18,19,22,30,32–34,41] As one of the members in the 2D MX_2 family, SnX_2 monolayers have been reported for applications in solar-driven water splitting, lithium battery, and field-effect transistor because of their semiconducting characteristic, rich abundance, and environment-friendly property.[35–42] Generally, transition metal dichalcogenides have hexagonal or rhombohedral symmetry, where the metal atoms have octahedral (1T) or trigonal prismatic (2H) coordination.[4] Experimentally, the two phases of a 2D MX_2 monolayer can interchange with each other under suitable conditions. For example, WS_2 is energetically stable in the 2H phase, but 1T WS_2 can be realized in experiments.[43] Theoretical calculations have shown that 1T SnS_2 and $SnSe_2$ monolayers are indirect semiconductors.[35,41] Till date, most of the theoretical work only focuses on 1T SnX_2 structures because they are energetically stable. A theoretical study of their 2H structures is not available, but it is necessary to reveal their physical properties for possible applications. At the same time, the effects of hydrogenation and tension on their electronic properties, which may lead to potential applications, have not been studied. In this work, we systematically investigate the electronic properties of SnX_2 monolayers and present an easy and simple method to tune their properties by hydrogenation and tension. We show that their electronic properties strongly depend on the chalcogen atom in the compounds because of the bonding state between the Sn and X atoms. We further show that p-type/intrinsic semiconducting and metallic monolayers with tunable band gaps can be obtained by hydrogenation and applied tension.

II. Methods

We carry out first-principles calculations to study the electronic and magnetic properties of tin dichalcogenide monolayers with

[a] Institute of Applied Physics and Materials Engineering, Faculty of Science and Technology, University of Macau, Macao SAR, China. E-mail: huipan@umac.mo; Fax: +853 88222426; Tel: +853 88224427

[b] Department of Mechanical Engineering, Materials Science & Engineering Program, and Texas Materials Institute, The University of Texas at Austin, Austin, USA

† Electronic supplementary information (ESI) available. See DOI: 10.1039/c5tc00093a

hydrogenation and under tension on the basis of the density functional theory (DFT)[44] and Perdew–Burke–Ernzerhof generalized gradient approximation (PBE-GGA).[45] The Vienna ab initio simulation package (VASP)[46] with a projector augmented wave (PAW) scheme[47,48] is used. The Monkhorst–Pack scheme of *k*-point sampling[49] is used for integration over the first Brillouin zone. A 13 × 13 × 1 grid for *k*-point sampling for the geometry optimization of unit cells and an energy cut-off of 450 eV are consistently used in our calculations. Sufficiently large supercells are used so that the monolayers in the neighboring cells in the vertical direction (perpendicular to the monolayer) are separated by a vacuum region of at least 15 Å. A 2 × 2 × 1 cell is used to study the spin alignments. Both the spin-polarized/unpolarized calculations are employed. Good convergence is obtained with these parameters, and the total energy was converged to 2.0×10^{-5} eV per atom.

III. Results and discussion

3.1 Structural properties

In our calculations, we focus on 2H tin dichalcogenide monolayers (SnX_2, X = S, Se, and Te) and the effects of hydrogenation and tension on their electronic properties (Fig. 1a). The pure and hydrogenated SnX_2 monolayers are first optimized to obtain the lattice parameters. The hydrogenation is realized by putting hydrogen atoms on the top of X atoms at one surface (Fig. 1b) or both the surfaces (Fig. 1c) of SnX_2 monolayers, leading to the formation of a chemical bond (H–X). For a convenient discussion below, the pure, one-surface hydrogenated, and two-surface hydrogenated SnX_2 monolayers are named as SnX_2-*n*H-MLs with n = 0, 1, and 2, respectively. The external tension is statically applied to these monolayers by uniform biaxial in-plane stretching, which is defined as $\varepsilon = \frac{a - a_0}{a_0} \times 100\%$ (where a_0 and a are the lattice constants of the monolayers without and with tension, respectively). The lattice parameters of pure and hydrogenated SnX_2 monolayers are obtained from their fully optimized structures (Table 1). We can see that the lattice constant increases as X changes from S to Se; it increases further as X changes to Te due to the enhanced ionic bonding between the Sn and X atoms. At the same time, hydrogenation leads to the expansion of the lattices of SnX_2 monolayers (Table 1). The lattice constant of pure SnS_2 monolayer is 3.618 Å, which increases to 4.001 Å and 4.455 Å by hydrogenation on one surface and both the surfaces, respectively. Similarly, the lattices of $SnSe_2$ and $SnTe_2$ monolayers are extended by 11.3% and 17.8% for hydrogenation on one surface, respectively, and extended by 24.4% and 26.8% for hydrogenation on both the surfaces, respectively. The S–H bond lengths are about 1.365 and 1.354 Å for the SnS_2-1H and SnS_2-2H monolayers, respectively (S1a, ESI†). We see that the X–H bond increases as X changes from S to Se (S1b, ESI†), and it increases further as X changes to Te (S1c, ESI†). This bond length is longer in SnX_2-1H-ML than that in SnX_2-2H-ML (S1, ESI†). The relaxed structures of SnX_2-*n*H-MLs (n = 0, 1, and 2) under tension show that the Sn–X bond increases linearly and the X–X distance in the vertical direction (perpendicular to monolayer) decreases as the tension increases (Fig. 2), except the Sn–Te bond in the $SnTe_2$-0H-ML (Fig. 2e), which decreases as the tension increases from 0 to 6%, and increases as the tension further increases. Accompanying the change of the Sn–Te bond in $SnTe_2$-0H-ML, we see that the Te–Te distance in the vertical direction drops fast in a range from 0 to 6% (Fig. 2f). The change of the X–H bond is less than 0.5% under the range of tension (0 to 10%) (S1, ESI†). The hydrogenation and tension should affect the electronic properties of the SnX_2 monolayers due to the changes of their lattice parameters.

Table 1 The lattice parameters of SnX_2 monolayers with and without hydrogenation

		Lattice constant (Å)	∠X—Sn–X (°)
SnS_2	0H	3.618	75.473
	1H	4.001	67.134
	2H	4.455	59.678
$SnSe_2$	0H	3.799	76.308
	1H	4.229	66.599
	2H	4.726	58.135
$SnTe_2$	0H	3.799	88.855
	1H	4.476	68.784
	2H	4.819	63.128

3.2 Electronic properties of SnS_2 monolayers

To find out the ground states of SnX_2-*n*H-MLs (n = 0, 1, and 2) under the tension range from 0 to 10%, the energy differences between their anti-ferromagnetic and ferromagnetic states

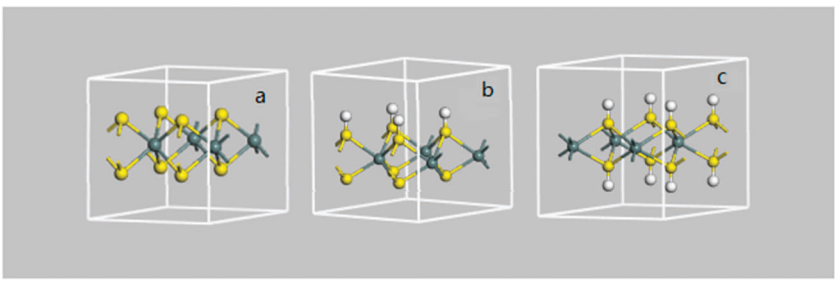

Fig. 1 The representative structures of (a) pristine SnX_2 (SnX_2-0H-ML), (b) SnX_2 with one surface covered by hydrogen atoms (SnX_2-1H-ML), and (c) SnX_2 with both its surfaces covered by hydrogen atoms (SnX_2-2H-ML).

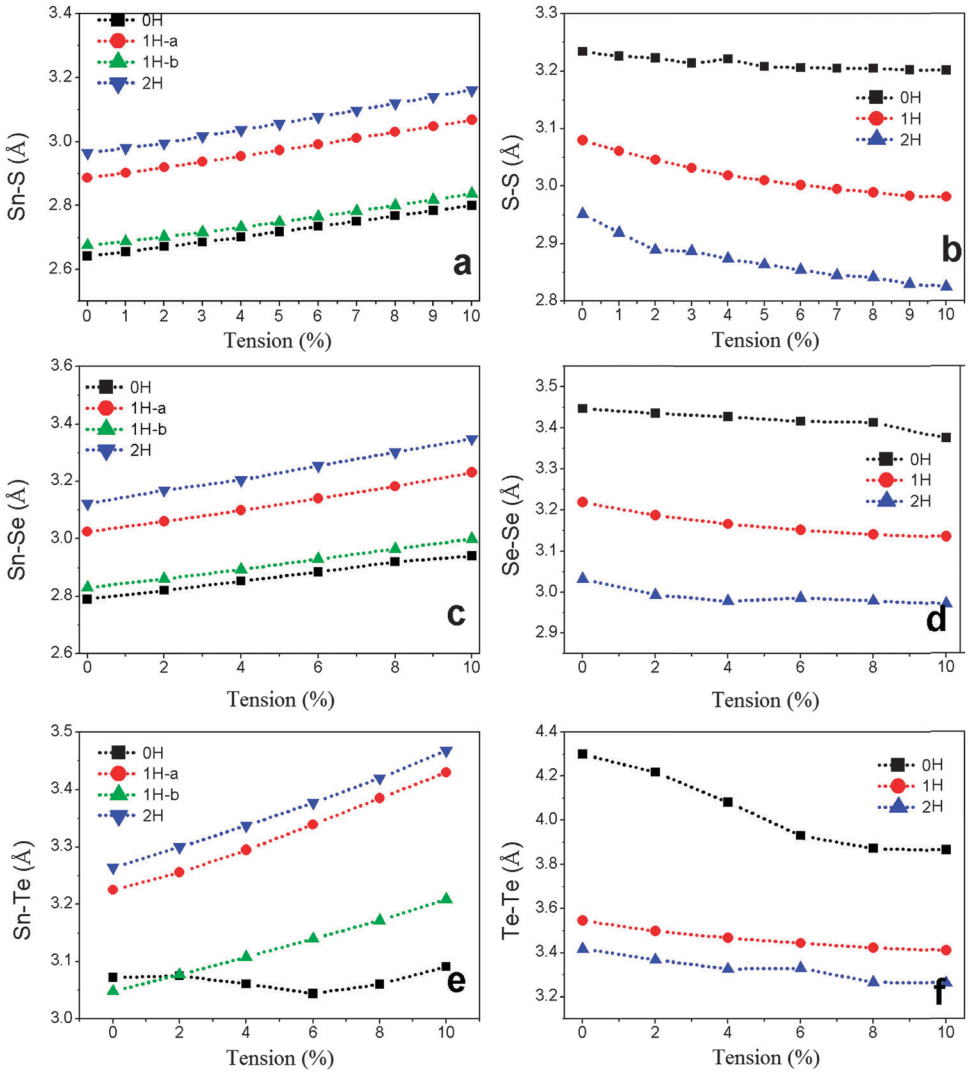

Fig. 2 The nearest atom-atom distance of (a) Sn–S, (b) S–S, (c) Sn–Se, (d) Se–Se, (e) Sn–Te, and (f) Te–Te. 1H-a and 1H-b refer to the bond lengths of Sn–X with and without H-coverage in SnX_2-1H-ML, respectively. X–X (X = S, Se, and Te) refers to the distance between two X atoms in the vertical direction (perpendicular to the monolayer).

(spin-polarization) are calculated. The ultra-small energy differences within ±1 meV show that these systems are non-magnetic (S2, ESI†). Therefore, we focus on spin-unpolarized calculations in the following discussion. The calculated band structure shows that SnS_2-0H-ML at $\varepsilon = 0$ is an indirect band semiconductor with a band gap of 0.78 eV, whose conduction band bottom (CBB) and valence band top (VBT) are at the *M* and *Γ* points in the first Brillouin zone, respectively (Fig. 3a). As the Fermi level is within the band gap, we see that SnS_2-0H-ML is an intrinsic semiconductor. The band gap of the 2H SnS_2 monolayer is about half that of 1T SnS_2.[41] The partial densities of states (PDOSs) show that its CBB is contributed by S-p and Sn-s states, and the VBT is dominated by S-p electrons (Fig. 3b). The CBB and VBT shift downward on the hydrogenated SnS_2 monolayers (Fig. 3c and e). We see that SnS_2-1H-ML is a p-type semiconductor because the Fermi level is within the valence band (when considering the up band as the conduction band) and has a band gap of 1.77 eV (Fig. 3c). When both the surfaces are hydrogenated (Fig. 1c), the VBT further moves downward and leaves the Fermi level within the band gap, leading to an intrinsic semiconductor with a gap of 1.88 eV (Fig. 3e). The PDOSs show that the VBTs of SnS_2-1H-ML and SnS_2-2H-ML are contributed by S-p and Sn-s electrons, and CBBs are dominated by Sn-p states (Fig. 3d and f). Comparing the band structures and PDOSs of pure SnS_2 monolayer and those with hydrogenation (Fig. 3), we see that the CBB of SnS_2 monolayer without hydrogenation (Fig. 3a and b) moves downward and becomes the VBT of the SnS_2 monolayer with hydrogenation (Fig. 3–f). We find that the pure SnS_2 monolayer (SnS_2-0H-ML) is an intrinsic semiconductor and its lowest conduction band is empty (Fig. 3a and b). When one side is fully covered by hydrogen atoms (SnS_2-1H-ML), one electron is donated to its lowest conduction band (or the band still holds one hole). Based on the Fermi–Dirac distribution, the Fermi level moves upward (or the lowest conduction band moves down) because the electrons can only occupy states below this level. If considering the band above the

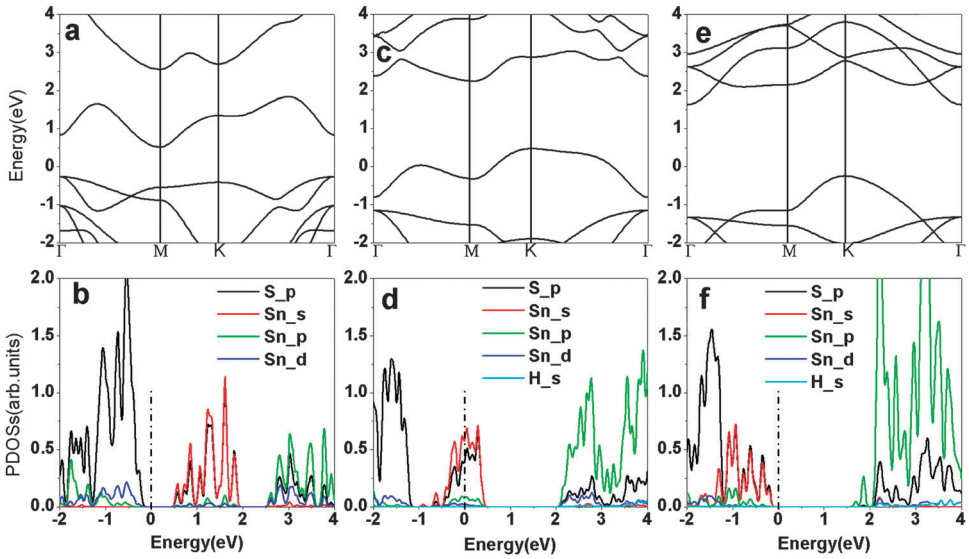

Fig. 3 Calculated band structures of (a) SnS_2-0H-ML, (c) SnS_2-1H-ML, and (e) SnS_2-2H-ML and partial density of states of (b) SnS_2-0H-ML, (d) SnS_2-1H-ML, and (f) SnS_2-2H-ML. Fermi level is at 0 eV.

Fermi level as a new conduction band bottom, SnS_2-1H-ML is a p-type semiconductor (Fig. 3c and d). When another side of the monolayer is also fully covered by hydrogen atoms (SnS_2-2H-ML), one more electron is donated to the lowest empty state. Now, the energy level holds two electrons and is saturated, leading to a further downward-movement (or the Fermi level moves further upward). Therefore, SnS_2-2H-ML is an intrinsic semiconductor (Fig. 3e and f). At the same time, we observe that hydrogenation leads to an extension of the lattice constant or tension on the lattice (Table 1). The tension may also affect their electronic properties accordingly.

To investigate the effect of tension, these monolayers are stretched statically in biaxial directions. Our calculations show that SnS_2-0H-ML has the maximal band gap (0.79 eV) at $\varepsilon = 1\%$, semiconducting characteristics at $\varepsilon \leq 8\%$, and metallic characteristics when $\varepsilon > 8\%$ (inset in Fig. 4a). The calculated band structures and PDOSs under tension reveal the origin of the trend (Fig. 3a, b and 5). We see that the conduction band of SnS_2-0H-ML at the Γ point in reciprocal space is pulled downward with the increase of tension (Fig. 5a) and becomes CBB when $\varepsilon = 4\%$ (Fig. 5c). At the same time, its valence band at the K point is pushed upward, resulting in a new VBT at $\varepsilon = 4\%$ (Fig. 5c). With further increasing tension, the CBB will touch (at $\varepsilon = 8\%$, Fig. 5e) and finally cross the Fermi level and overlap with the VBT (Fig. 5g), leading to metallic properties. The PDOSs show that the VBTs of strained SnS_2-0H-ML are still dominated by S-p electrons, and CBBs are mainly contributed by S-p and Sn-s states (Fig. 5b, d, f and h). Although hydrogenation also leads to the extension of the lattice constants (or tension) (Fig. 2), the effect of hydrogenation on the electronic properties (Fig. 3c–f) is totally different from that of external tension (Fig. 5), indicating that the observed electronic properties of SnS_2-1H-ML and SnS_2-2H-ML at zero tension are attributed to hydrogenation (Fig. 3c–f).

Besides the effect of tension on the electronic properties of SnS_2-0H-ML, we also investigate those on SnS_2-1H-ML and SnS_2-2H-ML. We see that the band gap of SnS_2-1H-ML increases fast to 1.855 eV at $\varepsilon = 2\%$, decreases with further increasing tension, and converges to 1.773 eV at $\varepsilon = 10\%$ (Fig. 4a). The calculated band structures and PDOSs show that the CBB of SnS_2-1H-ML at the M point is pushed upward fast, leading to an increased band gap in a tension range from 0 to 2% (Fig. 3c and d and 6a and b). When $\varepsilon > 2\%$, the CBB is at the Γ point and remains almost unchanged under tension, while the VBT at the K point is continuously pushed upward slowly, resulting

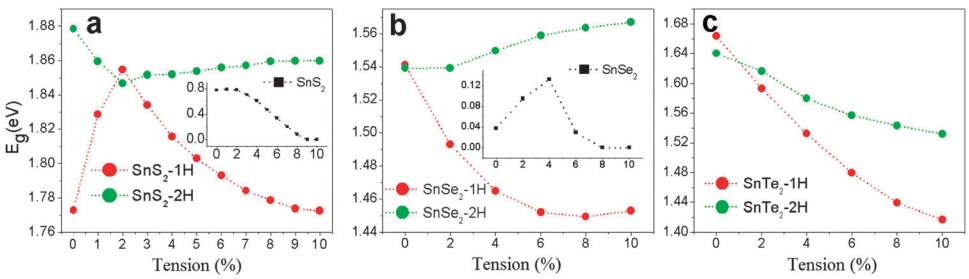

Fig. 4 Calculated band gaps of (a) SnS_2-nH-MLs, (b) $SnSe_2$-nH-MLs, and (c) $SnTe_2$-nH-MLs as a function of tension. n = 1 and 2. The insets in (a) and (b) show the calculated band gap of pure SnS_2 and $SnSe_2$ monolayers, respectively, as a function of tension.

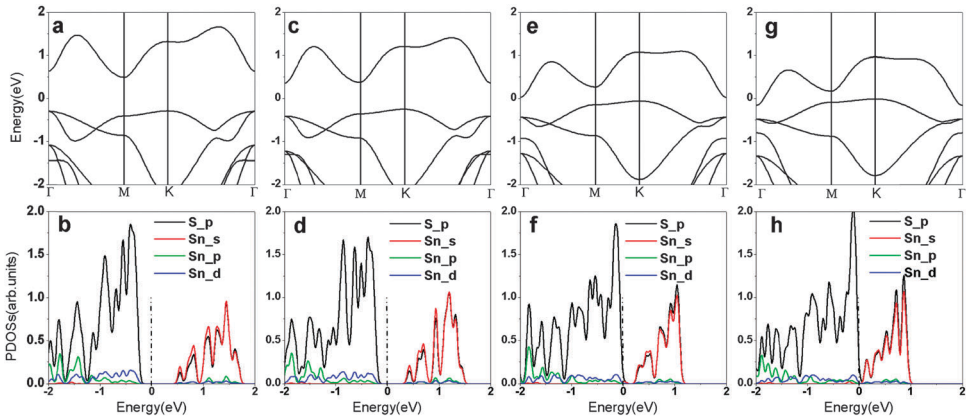

Fig. 5 Calculated band structures of SnS_2-0H-ML at tension of (a) 2%, (c) 4%, (e) 8% and (g) 10%, and partial density of states of at tension of (b) 2%, (d) 4%, (f) 8% and (h) 10%. Fermi level is at 0 eV.

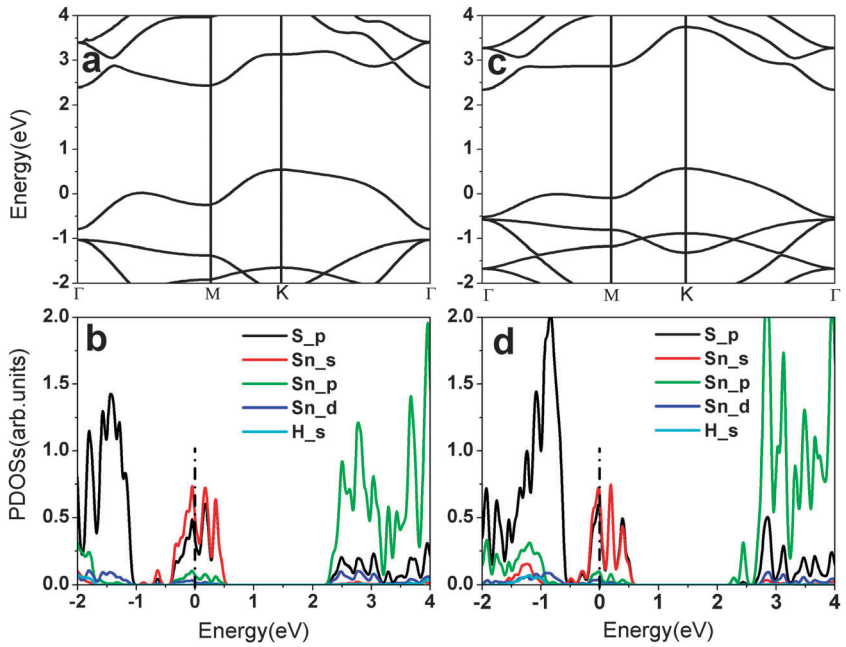

Fig. 6 Calculated band structures of SnS_2-1H-ML at tension of (a) 2% and (c) 10%, and partial density of states at tension of (b) 2% and (d) 10%. Fermi level is at 0 eV.

in a reduced band gap (Fig. 6c and d). The contribution to the VBT and CBB of SnS_2-1H-ML is unaffected by tension (Fig. 6b and d).

Different from SnS_2-1H-ML, the band gap of SnS_2-2H-ML decreases initially with tension and reaches the minimum (1.847 eV) at ε = 2% (Fig. 3a). Then, it increases slightly and converges to 1.86 eV with further increasing tension. The calculated band structures show that the CBB of SnS_2-2H-ML is pulled down when the tension increases from 0 to 2% (Fig. 3c and d and 7a and b), and its band gap reduces accordingly. When $\varepsilon > 2\%$, its CBB remains almost unaffected, while its VBT is pushed downward (Fig. 7c and d), leading to a slight increment of the band gap. When SnS_2-2H-ML is compared with SnS_2-0H-ML and SnS_2-1H-ML, we see that the lattice constant of SnS_2-2H-ML is much larger than those of SnS_2-0H-ML and SnS_2-1H-ML (Fig. 2). The bonding state in SnS_2-0H-ML is dominated by covalent coupling, which is weakened in SnS_2-1H-ML and SnS_2-2H-ML due to extended lattices. The tension can also play the same role in the change of bonding states. It should be more apparent in SnS_2-0H-ML because of the strong covalent bonding, but becomes weak in SnS_2-2H-ML because of the reduced covalent bonding. Therefore, we see that the effect of tension on the electronic properties of SnS_2-0H-MLs is stronger than those of SnS_2-1H-ML and SnS_2-2H-ML.

3.3 Electronic properties of $SnSe_2$ monolayers

The band structure of $SnSe_2$-0H-ML (Fig. 8a) looks similar to that of SnS_2-0H-ML with a narrowed band gap (Fig. 3a). $SnSe_2$-0H-ML is an indirect band semiconductor with CBB at the *M*

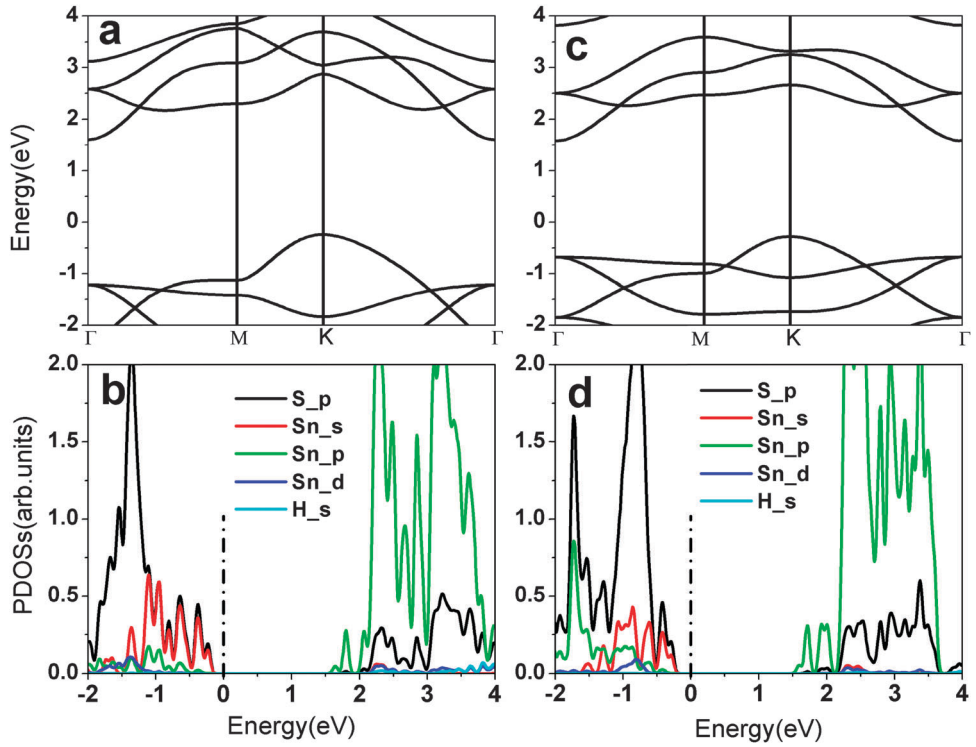

Fig. 7 Calculated band structures of SnS_2-2H-ML at tension of (a) 2% and (c) 10%, and partial density of states at tension of (b) 2% and (d) 10%. Fermi level is at 0 eV.

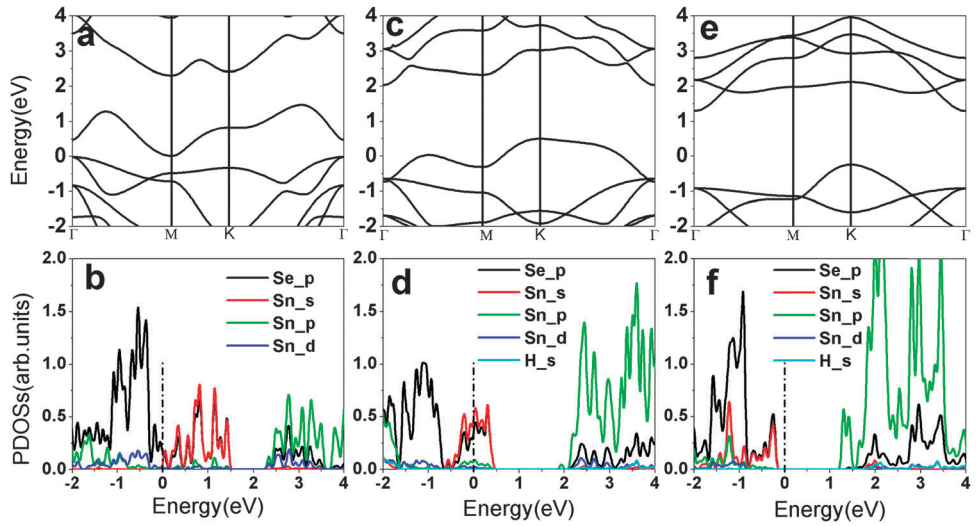

Fig. 8 Calculated band structures of (a) $SnSe_2$-0H-ML, (c) $SnSe_2$-1H-ML, and (e) $SnSe_2$-2H-ML, and partial density of states of (b) $SnSe_2$-0H-ML, (d) $SnSe_2$-1H-ML, and (f) $SnSe_2$-2H-ML. Fermi level is at 0 eV.

point and VBT at the Γ point and an ultra-narrow gap of 0.04 eV, which is much less than that of the 1T $SnSe_2$ monolayer.[35,41] Se-p electrons contribute to its VBT (Fig. 8b). Its CBB is dominated by Se-p and Sn-s states (Fig. 8b). Similar to the SnS_2 monolayer, hydrogenation leads to a change of the electronic properties of the $SnSe_2$ monolayer. With one surface fully covered by hydrogen atoms, $SnSe_2$-1H-ML becomes a p-type semiconductor with an indirect gap of 1.541 eV (Fig. 8c), where its VBT is contributed by Se-p and Sn-s electrons, and CBB by Sn-p states (Fig. 8d). When both the surfaces are hydrogenated, the monolayer becomes an intrinsic semiconductor with an indirect band gap of 1.539 eV (Fig. 8e and f). From the band structures of $SnSe_2$-nH-MLs (n = 0, 1, and 2), we can see that the CBB of $SnSe_2$-0H-ML (Fig. 8a) moves downward to become the VBTs of $SnSe_2$-nH-MLs (n = 1 and 2) (Fig. 8c and e), which is consistent with SnS_2-nH-MLs (Fig. 3).

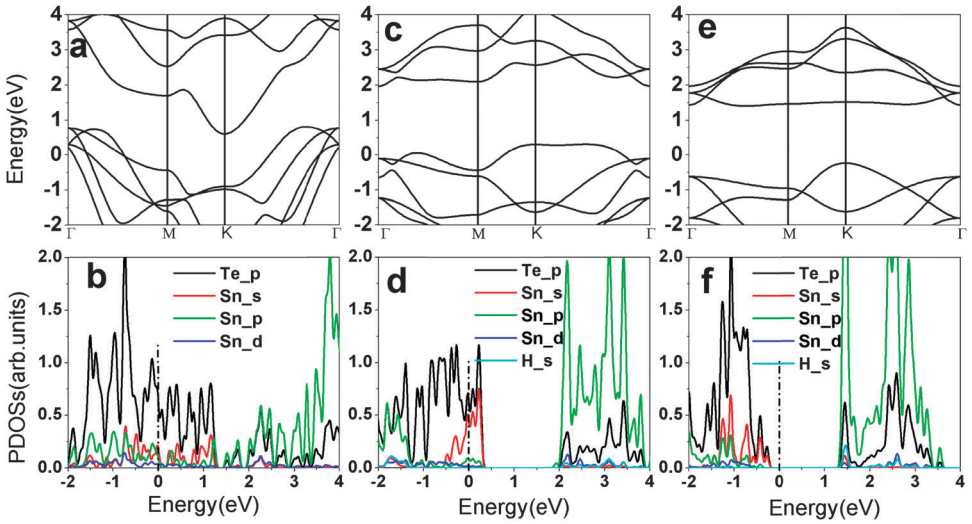

Fig. 9 Calculated band structures of (a) $SnTe_2$-0H-ML, (c) $SnTe_2$-1H-ML, and (e) $SnTe_2$-2 H-ML, and partial density of states of (b) $SnTe_2$-0H-ML, (d) $SnTe_2$-1H-ML, and (f) $SnTe_2$-2H-ML. Fermi level is at 0 eV.

When tension is applied to $SnSe_2$-*n*H-MLs, we see that their electronic structures are tuned (Fig. 4b). The band gap of $SnSe_2$-0H-ML starts to increase with the tension and reaches the maximum (0.133 eV) at ε = 4%, and it then decreases to zero with further increasing the tension (inset in Fig. 4b). The band structures show that its CBB (at the *M* point) of $SnSe_2$-0H-MLs under zero tension is pushed upward and transfers to the Γ point at ε = 4% (S3a and b, ESI†), leading to an increment of the band gap (inset in Fig. 4b). Further increasing the tension, its CBB (at the Γ point) is pulled downward (S3c and d, ESI†) and finally crosses over the valence band (S3e and f, ESI†), resulting in metallic characteristics. For $SnSe_2$-1H-ML, the reduction of its band gap is within 0.1 eV under tension from 0 to 10%, which is contributed by the downward-movement of CBB at the Γ point (S4, ESI†). The effect of tension on the band gap of $SnSe_2$-2H-ML is even smaller. The band gap of $SnSe_2$-2H-ML is only increased by $\sim$0.02 eV at ε = 10% (Fig. 4b). However, $SnSe_2$-2H-ML changes from an indirect band semiconductor to a direct semiconductor because the VBT changes from the *K* point to Γ point (S5, ESI†).

3.4 Electronic properties of $SnTe_2$ monolayers

Because of the relatively strong ionic bonding of Sn–Te compared to Sn–S and Sn–Se, $SnTe_2$-0H-ML is metallic (Fig. 9a and b). Similar to the previous discussion, it changes to a p-type semiconductor when one surface is hydrogenated (Fig. 9c and d), and an intrinsic semiconductor when both its surfaces are fully covered by hydrogen atoms (Fig. 9e and f). The VBTs of hydrogenated $SnTe_2$ monolayers are contributed by Te-p and Sn-s electrons and their CBBs, by Sn-p states (Fig. 9d and f). The metallic conductivity of $SnTe_2$-0H-ML is not affected by the applied tension because its Fermi level is maintained deep within the band (S6, ESI†). The band gaps of $SnTe_2$-1H-ML and $SnTe_2$-2H-ML are reduced by 0.3 and 0.1 eV, respectively, with the applied tension increasing from 0 to 10% (Fig. 4c). The reduction of the band gap of $SnTe_2$-1H-ML as the tension increases contributes to the downward-movement of CBB (S7, ESI†), while that of $SnTe_2$-2H-ML to the upward-movement of the VBTs at the Γ point, which yields a direct semiconducting characteristic (S8, ESI†).

IV. Conclusions

In summary, the electronic properties of SnX_2 monolayers and the effects of hydrogenation and tension are investigated by first-principles calculations on the basis of density-functional theory. Our calculations show that pure SnX_2 monolayers transfer from semiconductor to ultra-narrow band semiconductor, further to metal as X changes from S, to Se, and then to Te, because the covalent bond of Sn–X weakens in the same trend. Their electronic properties are strongly affected by hydrogenation and tension. Hydrogenation on one surface of the monolayers leads to a p-type semiconductor and that on both the sides of these monolayers results in an intrinsic semiconductor. At the same time, their band gaps are enlarged by hydrogenation. Pure SnS_2 and $SnSe_2$ monolayers can be tuned from a semiconductor to metal by applying tension. $SnSe_2$ and $SnTe_2$ monolayers with two surfaces covered by hydrogen atoms transfer from indirect to direct semiconductors under external tension as well as the reduction of band gaps. It is expected that multi-functional applications, such as sensors and nanodevices, may be achieved on the basis of tin dichalcogenide monolayers by hydrogenation and tension.

Acknowledgements

Hui Pan thanks the supports of the Science and Technology Development Fund from Macao SAR (FDCT-068/2014/A2), and Multi-Year Research Grant (MYRG2014-00159-FST) and Start-up Research Grant (SRG-2013-00033-FST) from Research & Development Office at University of Macau. The DFT calculations were performed at High Performance Computing Cluster (HPCC) of Information and Communication Technology Office (ICTO) at University of Macau.

References

1 K. S. Novoselov, A. K. Geim, S. V. Morozov, D. Jiang, Y. Zhang, S. V. Dubonos, I. V. Grigorieva and A. A. Firsov, *Science*, 2004, **306**, 666–669.
2 X. J. Zhou, J. L. Qiao, L. Yang and J. J. Zhang, *Adv. Energy Mater.*, 2014, **4**, 1301523.
3 X. L. Bao and K. P. Loh, *ACS Nano*, 2012, **6**, 3677–3694.
4 M. Chhowalla, H. S. Shin, G. Eda, L. J. Li, K. P. Loh and H. Zhang, *Nat. Chem.*, 2013, **5**, 263–275.
5 E. W. K. Koh, C. H. Chiu, Y. K. Lim, Y. W. Zhang and H. Pan, *Int. J. Hydrogen Energy*, 2012, **37**, 14323–14328.
6 Y. Ding, Y. L. Wang, J. Ni, L. Shi, S. Q. Shi and W. H. Tang, *Physica B*, 2011, **406**, 2254–2260.
7 W. X. Gu, J. Y. Shen and X. Y. Ma, *Nanoscale Res. Lett.*, 2014, **9**, 100.
8 T. R. Lin, L.-S. Zhong, Z. P. Song, L. Q. Guo, H. Y. Wu, Q. Q. Guo, Y. Chen, F. F. Fu and G. N. Chen, *Biosens. Bioelectron.*, 2014, **62**, 302–307.
9 H. Pan, *Sci. Rep.*, 2014, **4**, 7524.
10 L. T. Gew and M. Misran, *Nanoscale Res. Lett.*, 2014, **9**, 218.
11 Y. Lu and B. Yan, *J. Mater. Chem. C*, 2014, **2**, 5526–5532.
12 L. Newton, T. Slater, N. Clark and A. Vijayaraghavan, *J. Mater. Chem. C*, 2013, **1**, 376–393.
13 W. X. Feng, Y. G. Yao, W. G. Zhu, J. J. Zhou, W. Yao and D. Xiao, *Phys. Rev. B: Condens. Matter Mater. Phys.*, 2012, **86**, 165108.
14 H. Pan, *J. Phys. Chem. C*, 2014, **118**, 13248–13253.
15 H. Zhang, L. M. Liu and W. M. Lau, *J. Mater. Chem. A*, 2013, **1**, 10821–10828.
16 J. Feng, X. Sun, C. Wu, L. Peng, C. Lin, S. Hu, J. Yang and Y. Xie, *J. Am. Chem. Soc.*, 2011, **133**, 17832–17838.
17 D. Q. Gao, Q. X. Xue, X. Z. Mao, W. X. Wang, Q. Xu and D.-S. Xue, *J. Mater. Chem. C*, 2013, **1**, 5909–5916.
18 Y. Ma, Y. Dai, M. Guo, C. Niu, Y. Zhu and B. Huang, *ACS Nano*, 2012, **6**, 1695–1701.
19 Y. G. Zhou, Z. G. Wang, P. Yang, X. T. Zu, L. Yang, X. Sun and F. Gao, *ACS Nano*, 2012, **6**, 9729–9736.
20 Y. Jing, Z. Zhou, C. R. Cabrera and Z. F. Chen, *J. Phys. Chem. C*, 2013, **117**, 25409–25413.
21 D. Xiao, G. B. Liu, W. X. Feng, X. D. Xu and W. Yao, *Phys. Rev. Lett.*, 2012, **108**, 196802.
22 H. Pan, *Sci. Rep.*, 2014, **4**, 5348.
23 S. K. Panda, I. Dasgupta, E. asioglu, S. Blugel and D. D. Sarma, *Sci. Rep.*, 2013, **3**, 2995.
24 D. Z. Wang, Z. Pan, Z. Z. Wu, Z. P. Wang and Z. H. Liu, *J. Power Sources*, 2014, **269**, 229–234.
25 V. Sorkin, H. Pan, H. Shi, S. Y. Quek and Y. W. Zhang, *Crit. Rev. Solid State Mater. Sci.*, 2014, **36**, 319–367.
26 M. L. Tsai, S. H. Su, J. K. Chang, D. S. Tsai, C. H. Chen, C. I. Wu, L. J. Li, L. J. Chen and J. H. He, *ACS Nano*, 2014, **8**, 8317–8322.
27 N. J. Huo, S. X. Yang, Z. M. Wei, S. S. Li, J. B. Xia and J. B. Li, *Sci. Rep.*, 2014, **4**, 5209.
28 X. F. Song, J. L. Hu and H. B. Zeng, *J. Mater. Chem. C*, 2013, **1**, 2952–2969.
29 H. Pan and Y. W. Zhang, *J. Mater. Chem.*, 2012, **22**, 7280–7290.
30 L. Dong, R. R. Namburu and T. P. ORegan, *J. Mater. Sci.*, 2014, **49**, 6762–6771.
31 Y. Z. Wang, B. L. Wang, R. Huang, B. L. Gao, F. J. Kong and Q. F. Zhang, *Physica E*, 2014, **63**, 276–282.
32 H. Pan and Y. W. Zhang, *J. Phys. Chem. C*, 2012, **116**, 11752–11757.
33 H. Shi, H. Pan, Y. W. Zhang and B. I. Yakobson, *Phys. Rev. B: Condens. Matter Mater. Phys.*, 2013, **88**, 205305.
34 A. Kumar and P. K. Ahluwalia, *Physica B*, 2013, **419**, 66–75.
35 Y. C. Huang, C. Y. Ling, H. Liu, S. Y. Wang and B. Y. Geng, *J. Phys. Chem. C*, 2014, **118**, 9251–9260.
36 C. X. Xia, Y. T. Peng, H. Zhang, T. X. Wang, S. Y. Wei and Y. Jia, *Phys. Chem. Chem. Phys.*, 2014, **16**, 19674.
37 Y. Sun, H. Cheng, S. Gao, Z. Sun, Q. Liu, F. Lei, T. Yao, J. He, S. Wei and Y. Xie, *Angew. Chem., Int. Ed.*, 2012, **51**, 8727–8731.
38 P. Chen, Y. Su, H. Liu and Y. Wang, *ACS Appl. Mater. Interfaces*, 2013, **5**, 12073–12082.
39 H. S. Song, S. L. Li, L. Gao and Y. Xu, *Nanoscale*, 2013, **5**, 9666.
40 X. An, J. C. Yu and J. W. Tang, *J. Mater. Chem. A*, 2014, **2**, 1000–1005.
41 D. M. Guzman and A. Strachan, *J. Appl. Phys.*, 2014, **115**, 243701.
42 Y. Huang, E. Sutter, J. T. Sadowski, M. Cotlet, O. L. A. Monti, D. A. Racke, M. R. Neupane, D. Wickramaratne, R. K. Lake, B. A. Parkinson and P. Sutter, *ACS Nano*, 2014, **8**, 10743–10755.
43 D. Voiry, H. Yamaguchi, J. W. Li, R. Silva, D. C. B. Alves, T. Fujita, M. W. Chen, T. Asefa, V. B. Shenoy, G. Eda and M. Chhowalla, *Nat. Mater.*, 2013, **13**, 850–855.
44 P. Hohenberg and W. Kohn, *Phys. Rev.*, 1964, **136**, B864–B871.
45 P. E. Blöchl, *Phys. Rev. B: Condens. Matter Mater. Phys.*, 1994, **50**, 17953–17979.
46 G. Kresse and J. Furthmuller, *Phys. Rev. B: Condens. Matter Mater. Phys.*, 1996, **54**, 11169–11186.
47 J. P. Perdew, K. Burke and M. Ernzerhof, *Phys. Rev. Lett.*, 1996, **77**, 3865–3868.
48 G. Kresse and D. Joubert, *Phys. Rev. B: Condens. Matter Mater. Phys.*, 1999, **59**, 1758–1775.
49 H. J. Monkhorst and J. Pack, *Phys. Rev. B: Condens. Matter Mater. Phys.*, 1976, **13**, 5188–5192.